Journal of Physics D:
Applied Physics

PAPER

Comparison of direct and transferred cold atmospheric discharge in long, flexible tubes for the decontamination and removal of *Pseudomonas aeruginosa* biofilms

To cite this article: Antoine Remy *et al* 2026 *J. Phys. D: Appl. Phys.* **59** 025211

Journal of Physics D: Applied Physics

PAPER

RECEIVED
8 September 2025

REVISED
22 December 2025

ACCEPTED FOR PUBLICATION
2 January 2026

PUBLISHED
9 January 2026

Comparison of direct and transferred cold atmospheric discharge in long, flexible tubes for the decontamination and removal of *Pseudomonas aeruginosa* biofilms

Antoine Remy[1,*], Juliette Zveny[2], Teo Serra[1], Amélie Bourgeois[3], Orianne Bastin[1], Dalila Lakhloufi[4], Arnaud Lemmers[3], Anne Botteaux[4], Alain Delchambre[1], Francois Reniers[2] and Antoine Nonclercq[1]

[1] Bio-, Electro- and Mechanical- Systems (BEAMS), Biomed Group, Ecole polytechnique de Bruxelles, Brussels, Belgium
[2] Chemistry of Surfaces, Interfaces, and Nanomaterials, ChemSIN, Université Libre de Bruxelles, Faculty of Sciences, Brussels, Belgium
[3] Laboratory of Experimental Gastroenterology, Université Libre de Bruxelles (ULB), Faculty of Medicine, Brussels, Belgium
[4] Laboratory of Microbiology, European Plotkin Institute for Vaccinology (EPIV), Université Libre de Bruxelles (ULB), Faculty of Medicine, Brussels, Belgium
[*] Author to whom any correspondence should be addressed.

E-mail: antoine.remy@ulb.be

Keywords: biofilms, DBD, FTIR, non-thermal discharge, decontamination, plasma medicine

Abstract

Endoscope working channels are particularly vulnerable to bacterial contamination and biofilm formation due to repeated exposure to biological fluids and limited sterilization options. Inadequate reprocessing can lead to the formation of persistent biofilms and the transmission of healthcare-associated infections. To address this, we investigate the use of cold atmospheric plasma (CAP) generated directly inside endoscope-like Polytetrafluoroethylene (PTFE) tubing to improve decontamination and biofilm removal. This study compares two dielectric barrier discharge (DBD) configurations: a one discharge tube (ODT), in which the plasma is generated directly inside the contaminated tube, and a two discharge tube (TDT), where a high-power upstream discharge supplies reactive species to a second discharge within the tube, also called transferred discharges. Both systems were evaluated using 2 cm samples of PTFE tube colonized with *Pseudomonas aeruginosa* biofilms, using the Pineau-Alfa model. Several gases or gas mixtures (He, Ar, He/O_2, Ar/H_2O, He/H_2O, and air) were tested. The discharges were characterized using electrical measurements, optical emission spectroscopy, Fourier transform infrared spectroscopy FTIR, and H_2O_2 quantification to analyze the production of reactive oxygen and nitrogen species (RONS). All gas conditions except TDT–air achieved full bacterial decontamination within 5 min. However, biofilm removal was limited, with the most effective condition (ODT–He/H_2O) reducing biofilm coverage on the surface by 29 $\pm$ 6%. The ODT configuration provided superior local RONS delivery, including atomic oxygen and OH radicals. Its simpler design and the direct contact of the discharge with the contaminated surfaces present significant advantages for implementation in clinical settings, while maintaining the same decontamination capabilities. These findings confirm the feasibility of CAP-based *in-situ* decontamination for long, flexible medical tubing. Further optimization of discharge parameters and treatment time is required to enhance biofilm removal and achieve single-step, residue-free reprocessing of endoscopic devices while eliminating the reliance on hazardous chemicals (e.g. ethylene oxide, glutaraldehyde) or disposable endoscopes.

1. Introduction

The USA Centre for Disease Control indicates that endoscopes are the medical device responsible for most healthcare-associated infections [1]. Due to their complex structure composed of various channels, endoscopes cannot be thoroughly sterilized. In particular, the so-called biopsy or working channel

allows tools to be inserted into the patient [2]. They are disinfected using dedicated cleaning equipment [1], but it remains unsatisfactory, particularly for complex endoscopes such as duodenoscopes and therapeutic echoendoscopes [3, 4]. The working channel's inner surface is made of polytetrafluoroethylene (PTFE) because of its good chemical and biological inertness. However, the use and successive insertion of metallic tools create surface irregularities that, with insertion and usage, promote the biofilm's adhesion and build up [4].

Biofilms are 3D-multilayered structures (matrix) built by bacteria and made of polysaccharides, deoxyribonucleic acid, and proteins. They protect bacteria from external aggression or environmental stresses and provide a safe growing medium for the bacterial colony [5]. In medical device disinfection, where bacteria and biofilms must be removed from devices, biofilms pose a major challenge due to the poor penetration of detergents into the matrix [5]. This is especially true, as the survival and regrowth of bacteria through successive cleaning and usage cycles select resistant bacteria. Multiple-use surgical instruments, mainly endoscopes, containing electronics and various polymeric parts, are particularly prone to biofilm infections because they cannot be reprocessed in a high-temperature autoclave [6]. It has been shown that bacteria embedded inside biofilms are 10–100 times more resistant to endoscope washing than planktonic, or 'free,' bacteria [4]. Endoscopy techniques do not require a surgical incision to enter the gastrointestinal tract, which effectively reduces the risk of infection. However, the patient can undergo post-operation infections [2, 4, 7–9].

Multiple new approaches have been developed to fully decontaminate endoscopes. Many are based on aggressive chemicals, such as peroxides or ethylene oxide gases. However, they pose new challenges to the cleaning personnel and can corrode metallic parts inside the device [10]. The industry's answer to the challenge is to develop new single-use endoscopes *de facto* solving the contamination problem but increasing the environmental impact of the healthcare sector [11].

A concurrent approach utilizes the bactericidal and reactive properties of non-thermal discharges, commonly referred to as 'Cold Atmospheric Plasma' (CAP). In a CAP, the electric field, ultraviolet radiation, and energetic species, known as reactive oxygen and nitrogen species (RONS), react and interact with biological matter, producing the biocidal effect. RONS are essential, as they trigger multiple stresses in the bacterial colony and react with the biofilm to degrade it, creating a toxic environment for the bacteria [12]. Numerous studies have attempted to utilize CAP to treat biofilms on flat surfaces or in a tube. We can distinguish four different approaches: indirect treatments using plasma-activated water (PAW) [13, 14], direct treatments using plasma jets [15, 16] or surface dielectric barrier discharge (DBD) [17, 18], plasma jets generated in a tube [19, 20], and finally, the approach studied in our previous work and in the present work, a DBD generated directly in a contaminated tube [21, 22].

The approach of using a plasma jet or a flat DBD directed toward a bacterial biofilm has been more thoroughly studied. Numerous studies have reported effective decontamination and biofilm etching in some cases [15–18]. It is common for CAP applications of this type to exhibit higher efficacy than PAW, which is attributed to the direct action of CAP reactive species (RONS, UV, etc.) on bacteria and biofilms [23].

To address the challenges of endoscope contamination, a plasma jet has been generated directly into a small-diameter PTFE tube. Notably, Bhatt *et al* [19] and Hervé *et al* [20] used a CAP plasma jet generated in Ar to decontaminate long PTFE tubes from bacteria or prions. The first study, which focused on small samples placed away from the jet, showed complete decontamination and removal of short (2 cm) biofilm sample in less than 10 min of CAP treatment. In contrast, the second study, which focused on long samples (2.2 m), demonstrated that the removal of prions was effective only when applied in combination with a liquid enzymatic treatment. They noted that the CAP only extended to 20 cm in the tube and that the gas was displacing the proteins towards the end of the tube (downflow).

Our approach for decontaminating and removing bacterial biofilms from long, narrow PTFE tubes is to generate CAP directly inside and through the tube using a DBD configuration. This approach provides direct and complete contact of the CAP with the inner surface of the entire tube. We have previously described this approach in two articles, one discussing its effect on PTFE and the other examining its biofilm removal capability [21, 22]. To remove biofilm from the tube surface, rather than relying on mechanical action or a liquid solution containing oxidative chemicals, we use physical etching. The etching of biofilms by discharge produces volatile compounds (CO_2, CO, H_2O …) from the biomaterial, a process known as mineralization. Due to ozone's high oxidation potential (2.07 V [24]), it can react with biomaterials via ozonation, leading to the release of carbon dioxide [25]. However, mineralization is known to be slow with ozone alone and usually requires the addition of a catalyst (or UV light) to produce OH radicals from O_3 and water, thereby increasing the mineralization rate [24, 26, 27]. The other active species is atomic oxygen, which is known to be an effective etching agent [28]. Due to its higher

oxidation potential (2.42 V) and simpler reaction mechanisms with biomaterials, the mineralization rate is higher than that of ozone [26, 29].

To reduce and optimize the treatment time for biofilm removal and decontamination, this study compares a system with one discharge in a tube (one discharge tube or ODT) and a system with two consecutive discharges in two consecutive tubes (two discharge tube or TDT), also known as transferred plasma in the literature [30, 31]. The ODT consists of a single discharge generated in the PTFE tube to be treated and directly powered by the generator. The TDT, on the other hand, has a high-power-density discharge generated upstream from the treated tube, which then transfers the power to a second discharge that is generated similarly to the ODT, in the treated tube. The first discharge produces a high amount of RONS before the second discharge, which has a lower power density but is in direct contact with the inner surface of the PTFE tube. We have generated discharges for both devices in various gas mixtures, including argon (Ar), helium (He), water-saturated argon (Ar/H_2O) and helium (He/H_2O), air, and oxygen in helium (He/O_2). The effects of those mixtures have been studied in a similar reactor design, with a focus on the degradation of the tube inner surface [22]. They concluded that the material degradation was minimal and that the effects were mainly oxidation of the surface by oxygen and hydroxyl radicals, along with an increase in roughness due to preferential etching of the amorphous PTFE in the case of oxygen-containing plasmas (Ar/O_2, Ar/H_2O, He/H_2O, and Air). Moreover, the maximum etching rate, measured around 50 μg min^{-1}, was found to be negligible over the total lifetime of an endoscope.

The gas mixtures were selected for their ability to produce various RONS. Water-saturated helium or argon discharges generate OH radicals, which react with each other to form H_2O_2. Oxygen in helium discharge mainly produces atomic oxygen (O) and ozone (O_3). Both are strong oxidants capable of degrading materials exposed to them, and have well-known disinfection capabilities. Finally, air discharge produces nitrogen oxides (NO, NO_2, NO_3, HNO_3, N_2O, and N_2O_5) and ozone, both of which are useful for decontamination and oxidation [23, 32]. The quantity of RONS produced should then reflect the disinfection capability. NO_x, O_3, and degradation products generated during discharge were monitored using Fourier transform infrared spectroscopy (FTIR). Spectrophotometric assay with $TiOSO_4$ was employed for H_2O_2 detection. Optical emission spectroscopy (OES) was utilized to monitor excited species in the tube (OH, Ar, He, N_2^*, …). The electrical parameters of the discharges were also closely studied (power dissipated, voltage amplitudes, and currents) to compare the TDT and the ODT under similar conditions.

To compare the decontamination capabilities of our two devices, we selected parameters that were tested similarly to those in our previous work [21]. A *Pseudomonas aeruginosa* (*P. aeruginosa)* biofilm was grown for 24 h in a PTFE tube to model a contaminated endoscope working channel. A small sample of the tube, placed in line with the tube discharge, was then treated. Twenty-four-hour regrowth assays were used to assess the tube decontamination, and crystal violet (CV) assays were used for biofilm removal efficacy.

2. Materials and methods

2.1. Plasma generation

This study is based on previous works that focused on generating and producing a plasma plume at the distal end of an endoscope working channel [33–38]. In their work, a plasma plume as large as possible was generated at the distal end of an endoscope to produce a discharge within the working channel of the endoscope.

Our CAP generator devices are based on the principle of DBDs set in a tubular disposition at atmospheric pressure. The dielectric of the DBD corresponds to the tube subjected to plasma treatment, and to replicate those present in endoscopes, we used a two-meter-long PTFE tube (1.5 × 3 mm ID × OD) with a metallic grounding sleeve tightly fitted around its exterior. These two components are characteristic of endoscope channel architecture and are essential for accurately simulating the conditions of a discharge within an actual endoscope channel. The components required to generate discharge in the tube are schematized in figure 1. More details on the two DBD reactors that we have developed (ODT and TDT) are provided in the following subsections and in figure 2.

The different gases used are all ALPHAGAZ 1 from Air Liquide. The flow rates are controlled by mass flow meters (MV-302, Bronkhorst). For the two gas mixtures with water vapor, the entire flow of gas (argon or helium) is fed into a water bubbler, which saturates the gas with water vapor. Table 1 summarizes the various gas characteristics and flow used and tested during this study. For the He/O_2 mixture, 50 ml min^{-1} of O_2 was added to the 1.5 l min^{-1} main Helium flow.

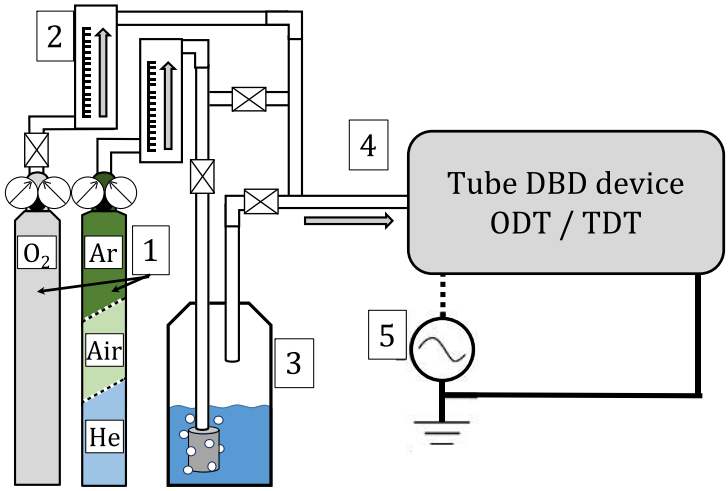

Figure 1. Schematic of the experimental setup. 1. Alphagas 1 cylinder; 2. Rotameter; 3. Water bubbler; 4. High-voltage feed through; 5. High-voltage AC power supply.

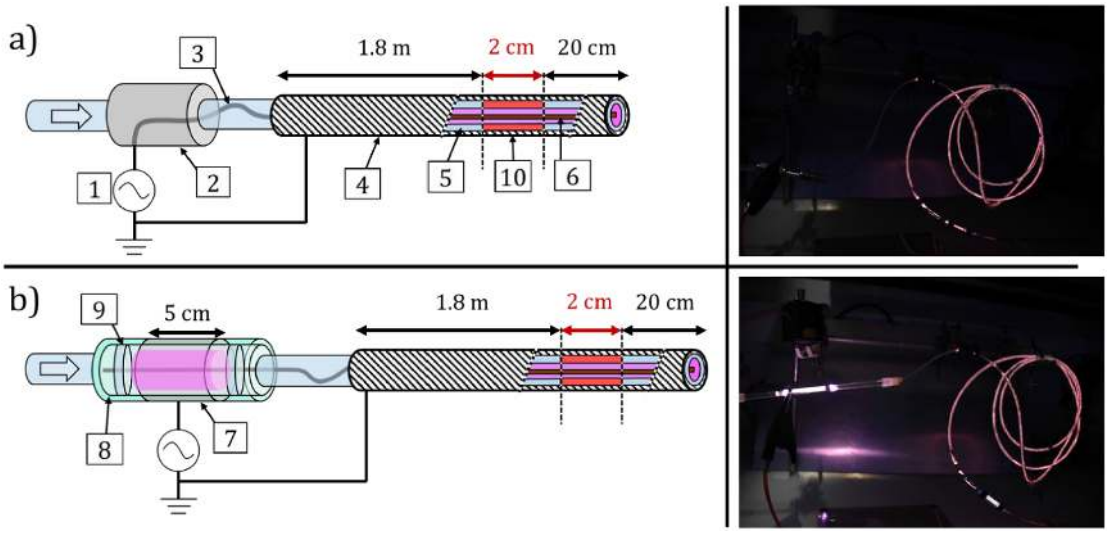

Figure 2. Schematic of the two devices with the gas inlet on the right, along with corresponding pictures of a helium discharge. (a) One-discharge tube (ODT). (b) Two-discharge tube (TDT). The red section corresponds to the position of the contaminated sample in the tube. 1, power supply; 2, high voltage feed through; 3, copper wire; 4, metallic braided sleeve; 5, PTFE tube; 6, discharge; 7, metallic mesh; 8, quartz tube; 9, spacer; 10, contaminated sample.

Table 1. Summary of the various gas mixtures used to generate the discharge.

Gas mix	Main gas flow rate (l min^{-1})	Secondary gas
Ar/H_2O	Ar–1.5	H_2O–20 mg $\cdot$ l^{-1}
Ar	Ar–1.5	/
He	He–1.5	/
He/O_2	He–1.5	O_2–3%$_{v/v}$
He/H_2O	He–1.5	H_2O–20 mg $\cdot$ l^{-1}
Air	Air–1.5	/

Two devices, shown in figure 2, were used to generate plasma. They are both cylindrical DBDs with gas flowing in the tube that forms the cylindrical DBDs. Both devices rely on the same basis: the high-voltage electrode is a 2 m-long, thin, flexible copper wire (Ø 0.35 mm/27 AWG) placed inside a PTFE tube and connected to a high-voltage AC power source. The counter or ground electrode is provided by a metallic braided sleeve (RS Components 821–1712) that is tightly fitted around the exterior of

the tube and connected to the electrical ground of the generator. This apparatus allows for the generation of a homogeneous discharge throughout the entire tube without causing blockage of the gas flow. Additionally, the high-voltage wire is easily insertable and removable from the tube, which is crucial for applying the system to an actual endoscope. The electrodes are powered by a sinusoidal high voltage, generating a plasma discharge in the tube at atmospheric pressure. The AC power supply consists of a frequency and power controller (AFS GT10S-V) and a high-voltage transformer (AFS GT30-1K). The selected frequency for the present study is 30 kHz for all tests.

2.1.1. ODT

The first system, schematized in figure 2(a), generates a discharge (6) confined inside the PTFE tube (5). The conductive wire (3) is directly connected to the AC power supply (1) using a stainless steel tube (2) connected to the PTFE tube. The metallic sleeve (4) around the PTFE tube provides the electrical ground. This design distributes the electrical power to the entire tube and can be used up to 15 W of power without excessive tube heating (less than 50 °C).

2.1.2. TDT

The second device (figure 2(b)) comprises two plasma discharges, generated by a set of 3 electrodes. The upstream discharge is generated in a 7 × 4 mm ID × OD quartz tube (8) with a 5 cm long metallic mesh (7) wrapped around the tube. This mesh is connected to the high-voltage generator (1). A thin stainless steel rod is placed inside the quartz tube, with ceramic spacers (9) used to keep it centered. The rod forms the second electrode of the system, and the upstream discharge is then confined between the metallic mesh and the stainless steel rod in a volume of approximately 0.7 cm^3. The rod is extended to the end of the quartz tube and connected to the copper wire in the same system as the ODT. The ODT part of the discharge generates a downstream discharge confined inside the PTFE tube. The complete assembly is called TDT. This design allows higher power to dissipate than the ODT (up to a total of 50 W), as most of the power is dissipated outside of the PTFE tube in the upstream discharge. It can be used up to 50 W.

The difference between the two apparatuses is the region where the discharge power is dissipated, and thus where the RONS and reactive elements, such as electrons, UV, and metastables, are produced. For the TDT, the upstream discharge has a higher energy density than the downstream discharge, and thus, it produces most of the species before the PTFE tube, which are then flushed into the PTFE tube. For the ODT, the energy is dissipated only in the PTFE tube, which is directly in contact with the contaminated areas.

2.2. Measurements of RONS in the gas state

An infrared absorption spectroscopy analysis using FTIR spectrometer (Bruker Vertex 70 V) was used to identify and quantify the RONS species produced in the gas during the discharge. The infrared light beam is redirected outside the spectrometer, passes through a homemade 200 mm optical path gas cell, and is collected by a DLaTGS detector. The gas output of the working channel discharge is directed into the gas cell. The concentrations of NO, NO_2, N_2O_5, N_2O, HF, CO, COF_2, and O_3 are extracted from the recorded infrared spectrum using the absorption cross-section of the HITRAN database [39]. The presence of CO_2 and H_2O in the spectra is due to the uncontrolled atmosphere around the gas cell, meaning that the qualitative and quantitative measurements of these two gases cannot be performed.

2.3. Electrical measurements

To measure the power dissipated by the two devices, we measured the voltage and current passing through each device. The voltage was measured using a high-voltage Tektronix P6015A probe, connected to the high-voltage generator. A 47 ohm shunt resistance was used to measure the current with a Rigol PVP2350 probe. All signals were acquired using a Rigol MSO5204 oscilloscope at 2.5×10^{-5} s time resolution. The power was then calculated by integrating the current and voltage over one period and then multiplying by the frequency. In the case of the TDT, two voltages were measured simultaneously: the voltage from the generator, which is applied to the quartz tube electrode, and the copper wire voltage inside the PTFE tube. To measure the voltage of the copper wire, a second high-voltage probe (P6015A) was added between the quartz tube and the PTFE tube.

2.4. Measurements of H_2O_2

Measurement of H_2O_2 production was performed using spectrophotometric titration. The titration utilizes the absorbance of a titanium complex, H_2TiO_4, at 410 nm, as measured using a UV–visible absorption spectrometer (UV-1650PC, Schimatzu). To measure the H_2O_2 produced by the discharge, 5 ml of a

solution of 7.0 g · l^{-1} of $TiOSO_4$ (Alfa Aesar 13825-74-6) dissolved in 1 M H_2SO_4 was placed in a small vessel (10 ml) and the output gases from the discharge were flowed in the vessel through a tube inserted in the top cap of the vessel and then out of the vessel by a second tube coming out of the cap. All the H_2O_2 formed in the discharge was assumed to react with the solution. Each measurement takes 10 min to increase the total amount of H_2O_2 measured and the absorbance of the solution. The total amount of H_2O_2 produced over 10 min of discharge was calculated from the concentration in the 5 ml solution, by using the known molar absorption coefficient of H_2TiO_4, 689 mol · l^{-1} · cm^{-1} from Machala *et al* [40]

2.5. Biofilm generation

The biofilm model is based on the Pineau-Alfa model [41]. The biofilm generation utilizes the growth of *P. aeruginosa* bacteria inside a PTFE tube. This process is extensively described in our previous publication [21]. It models the bacterial activity in an endoscope after successive utilizations.

The PTFE tube was filled with a solution of TSB (Tryptic Soy Broth [42]) containing 20 mg l^{-1} of ampicillin. Then the tube was inoculated with 10 ml of *P. aeruginosa* (PAO1) overnight culture (O/N 10^9–2.10^8 cfu ml^{-1}) diluted five times with TSB before injection. The inoculation consists of the recirculation of the solution for 20 min at a constant flow rate of 100 ml · min^{-1}. The growth phase lasted 24 h in a continuous flow of a new TSB solution at 3 ml · min^{-1} and 37 °C.

Before being used for the decontamination test, the contaminated PTFE tube was flushed with sterilized water and then with air at a low flow rate (less than 30 ml · min^{-1}) to stop biofilm growth. For all experiments, a 1.5 m long PTFE tube (3 × 5 mm ID × OD) was contaminated using this procedure, and then 2 cm long samples were cut for treatment. A 20 cm section at the beginning (upstream) of the 1.5 m long tube was avoided due to the presence of a thick biofilm.

2.6. OES

The emission spectrum of the discharge in the PTFE was recorded using an optical fiber-coupled spectrometer. The spectrometer is an Andor Shamrock 500 with an iDus-420 camera. The fiber was optically coupled to the discharge by placing it perpendicular to the PTFE tube in a 3D-printed holder, maintaining a distance of 1 cm between the fiber and the tube. The fiber was placed at the same position as the contaminated sample, around 20 cm before the end of the tube discharge. Thanks to the optical properties of PTFE, the discharge was observed directly through the PTFE tube between 200 nm and 900 nm.

2.7. Biofilm treatment

A configuration was established that combines plasma generation with biofilm presence to assess the efficacy of plasma-generated species on biofilms, as depicted in figure 2. Downstream of the tube, a section of the uncontaminated PTFE tube was substituted with a 2 cm section of 3 mm inner diameter PTFE tube containing the biofilm. The contaminated sample was then treated with plasma by passing the high-voltage electrode inside the tube.

For each treatment, three replicas were performed and analyzed separately. An additional control sample with biofilm is set aside, without any treatment.

2.8. Biofilm and bacteria analysis

The methodology used in this study has been previously described in our previous publication [21] and will not be detailed here. The regrowth assay was used as a qualitative test for the presence of remaining viable bacteria after treatment. On the other hand, the CV assay was used to quantify the remaining biofilm. Before analysis, the exterior of the treated samples was first cleaned with an ethanol solution (70%). The sample was then divided into two halves (transversal cut, 2 × 1 cm) and further divided into two halves (longitudinal cut). Two longitudinal halves were used for regrowth test, and the other two were used for CV test. The regrowth test is adapted from Doern *et al* [43] and requires incubating the samples in a Falcon tube for 24 h with TSB at 37 °C and 5% CO_2. A sample was considered decontaminated if the optical density at 600 nm was null, and contaminated if the optical density was over 0.1. The violet crystal optical density at 540 nm reflects the quantity of biofilm on the surface of the sample [44]. For comparison between multiple sets of samples, all results are displayed as a percentage of biofilm on the surface, with the optical density of the control sample representing 100% biofilm on the surface.

In this work, a decontaminated sample is defined as one in which bacteria do not proliferate under optimal conditions, such as those established in the regrowth test, and the bacteria in the biofilm are no longer viable. A biofilm is the accumulation of biological matter in which bacteria have grown, and the treatment is designed to remove this matter from the surface of the tube physically. Therefore, the presence of biofilm on the surface, as identified by the CV test, is insufficient to determine whether the

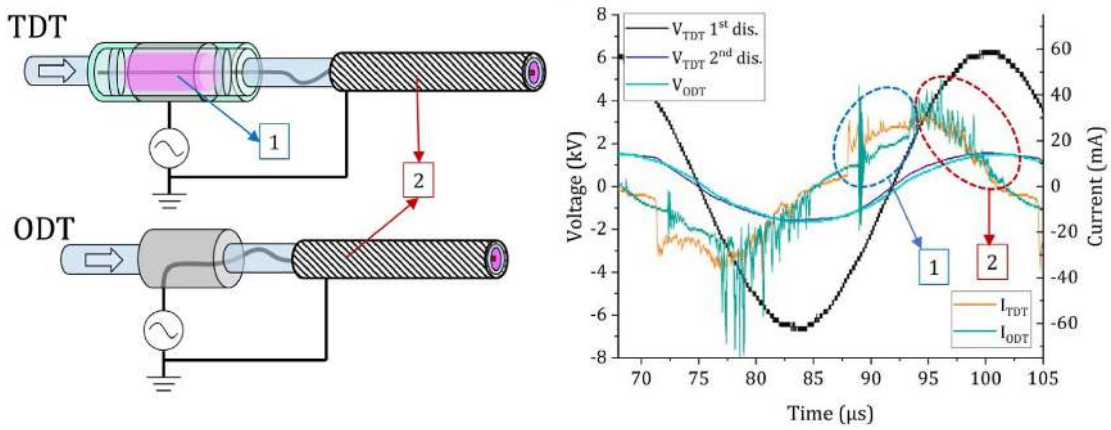

Figure 3. Voltage (kV) waveforms for the ODT (V_{ODT}) and TDT during the first (V_{TDT} 1st dis.) and second discharges (V_{TDT} 2nd dis.), along with the total current (mA) of the ODT (I_{ODT}) and TDT (I_{TDT}). The numbered labels indicate the discharge locations shown in the diagrams and their corresponding current waveforms: (1) discharge in the quartz tube of the TDT, and (2) discharge in the PTFE tube present in both devices.

sample has been decontaminated. The CV test is intended solely to evaluate the treatment's effectiveness in removing the biofilm. A sample exhibiting a complete absence of regrowth is deemed to be fully decontaminated, even in the presence of a biofilm and/or bacterial cells within the tube.

3. Results

3.1. Electrical characteristics

3.1.1. Current and voltage comparison between ODT and TDT in Ar/H_2O

Figure 3 compares the voltage and current of the ODT and the TDT discharges in Ar/H_2O. The voltage of the TDT first discharge is the voltage of the generator applied to the quartz tube, whereas the voltage of the ODT and the TDT second discharge is the voltage measured on the copper wire inside the PTFE tube. The ODT and the TDT are compared here in a configuration where the voltage of the ODT (V_{ODT}) matches exactly the voltage of the TDT second discharge (V_{TDT} 2nd dis. on the wire electrode). The current, on the other hand, is the total current passing through the system.

The Ar/H_2O discharge was selected as a representative case for the direct comparison between ODT and TDT configurations, as it clearly highlights the electrical differences between the two systems. Similar qualitative behaviors were observed for the other investigated gas compositions, as detailed in sections 3.1.2 and 3.1.3.

As can be seen, a clear difference is observed between the two TDT voltages (black and purple curves). The voltage of the second discharge is a combination of the capacitive coupling between the wire and the quartz electrode and the voltage drop during the discharge in the quartz tube. The latter is far less important than the former, and the waveform is mainly sinusoidal. In figure 3, in the first part (1) of I_{ODT}, a sharp current peak is recorded, which is probably due to an imperfect connection between the copper wire and the high-voltage generator, creating an artifact.

The current waveform of the TDT (I_{TDT}) displays two distinct discharge events: first, the quartz tube discharge circled in blue (1), characterized by a sharp, high-amplitude current peak, followed by a longer segment composed of multiple sharp and small current peaks closely spaced identified as microdischarges (2), circled in red. This type of double discharge has been discussed in a previously published work on helium discharge [45]; our system shares common electrical behavior. The second part of the discharge is attributed to the discharge in the PTFE tube. This interpretation is supported by the comparison with the ODT current waveform (I_{ODT}), which does not present any relevant current peak in the first part (1) of the discharge and then closely matches the second part (2) of the TDT signal, indicating that microdischarges primarily occur in the PTFE tube, similar to those in the ODT. A strong asymmetry is also observed between the positive and negative polarities, due to the asymmetry of our system. This asymmetry is due to the absence of a dielectric on the copper wire, which allows more current to flow in one direction than the other [46].

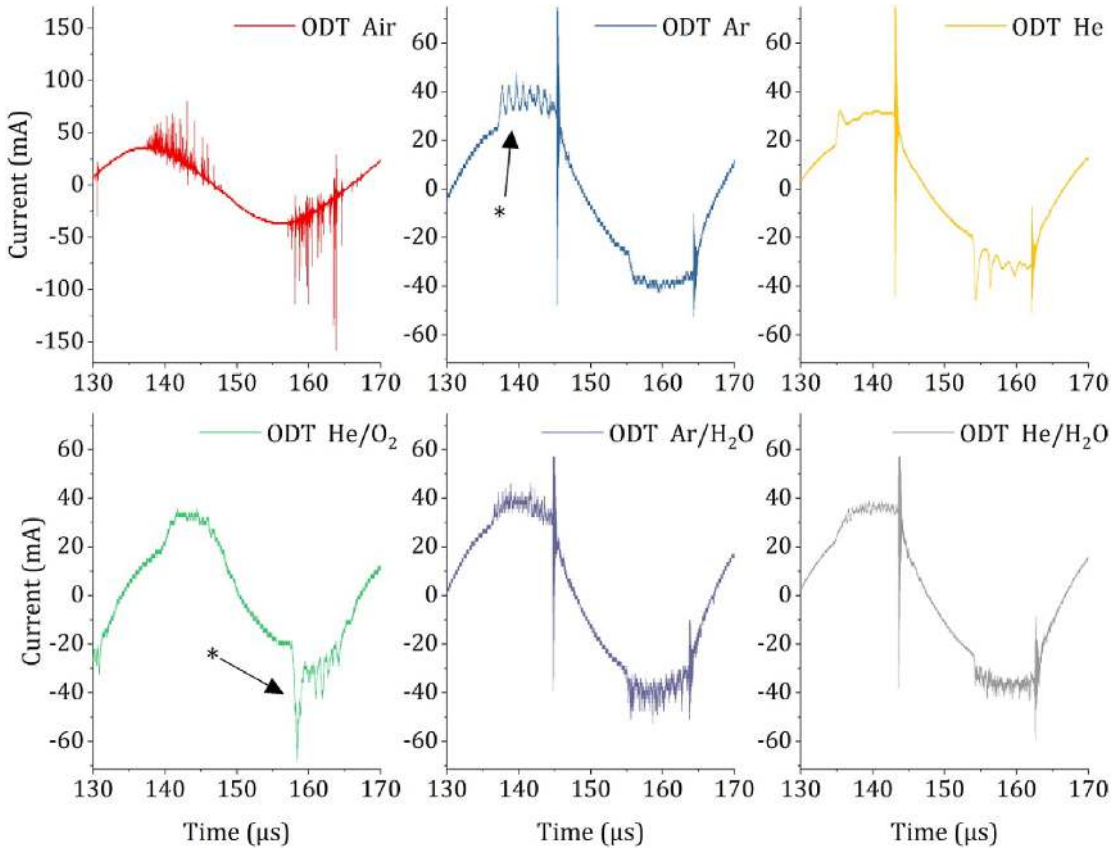

Figure 4. Comparison of the current (mA) during one period (30 kHz) in the ODT with air, Ar, He, He/O_2 (3%), Ar/H_2O, and He/H_2O gas mixture with a flow of 1.5 l min^{-1}. The strong and sharp current peak observed around 144 μs for Ar, He, Ar/H_2O, and He/H_2O can be attributed to an artifact of the measurement and, as such, should be disregarded.

3.1.2. Current distribution in the ODT in function of the gas

Figure 3 compares the current during one period in the ODT with air, Ar, He, He/O_2 (3%), Ar/H_2O, and He/H_2O gas mixture. For Ar, He, Ar/H_2O, a strong and sharp current peak is observed at 144 μs, which is a measurement artifact that should be disregarded. In figures 3 and 4, the microdischarges cannot be individually resolved and instead appear as densely packed current pulses characteristic of filamentary discharges [47].

The presence of microdischarges is observed in all gases except pure helium. In helium, it is well known that DBD at atmospheric pressure presents homogenous behavior instead of microdischarges, which is also observed here [48, 49]. Air, Ar/H_2O, and He/H_2O present similar microdischarges with small current peaks packed closely in the upper portion of the half period. On the other hand, He/O_2 and Ar exhibit strong current peaks in at least one polarity (highlighted by the star in figure 4), indicating stronger ionization of the gas.

3.1.3. Current distribution in the TDT

Figure 5 compares the current during one period in the TDT with the different gas mixtures. Similar behavior is observed for the TDT, with microdischarge in air, Ar, He/O_2, Ar/H_2O, and He/H_2O, but also in helium. In figure 5, we have highlighted the presence of the two discharge stages, which are observed for all gases except air. In air, the high current peak at the beginning is completely missing; instead, a large number of microdischarges with current peaks as high as 300 mA are observed throughout the entire discharge. They are also less closely packed than those observed for other gases or for the ODT. The polarity asymmetry is also observed, with a higher current peak in one polarity than the other.

3.1.4. TDT-ODT power consumption

Figure 6(a) compares the power consumed by the TDT 1st discharge (kV) as a function of the peak-to-peak voltage ($Voltage_{pp}$) measured on the first electrode (quartz tube) for various gas discharges in the TDT. This power is calculated by subtracting the power of the second discharge from the total power. The power varies considerably across the various gases at a given voltage. Particularly, the air discharge

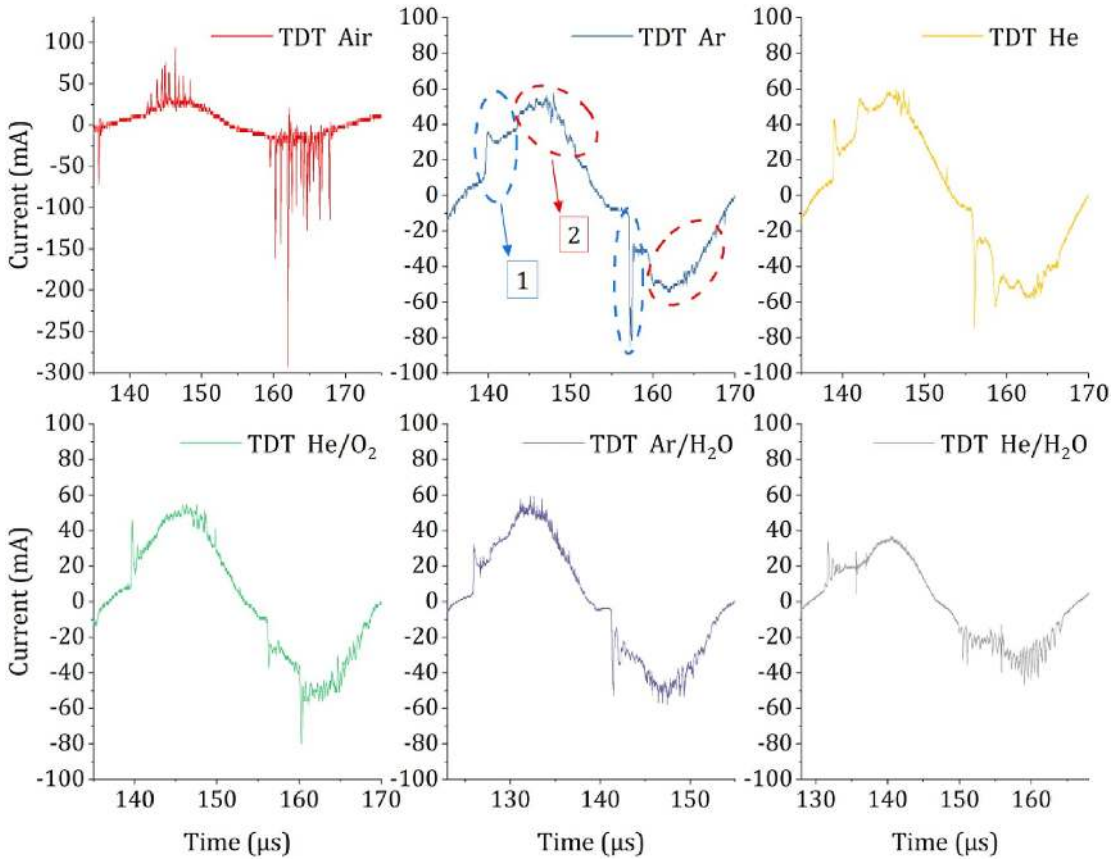

Figure 5. Comparison of the current (mA) during one period (30 kHz) in the TDT with air, Ar, He, He/O_2, Ar/H_2O, and He/H_2O gas mixture with a flow of 1.5 l · min^{-1}. (1) Large current peak corresponding to the first discharge in the quartz tube. (2) Microdischarges corresponding to the second discharge in the PTFE tube.

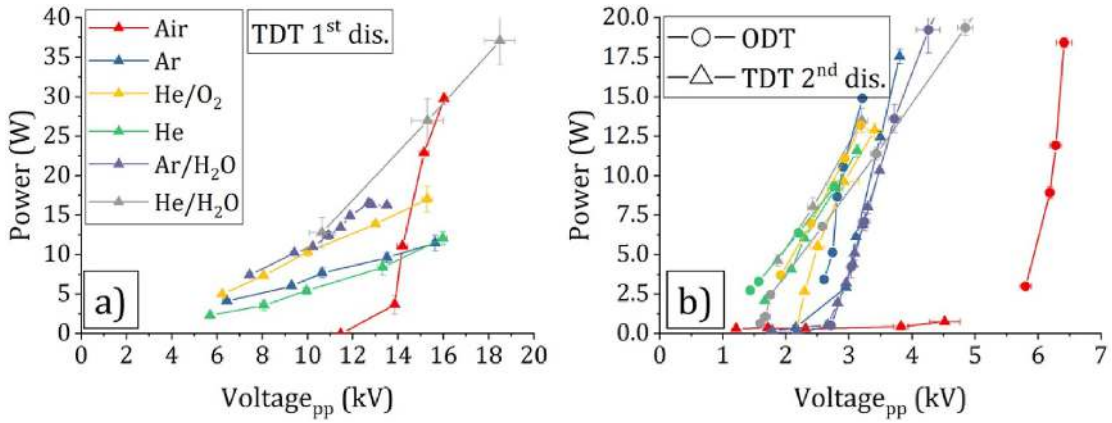

Figure 6. Power dissipated (W) over peak to peak voltage applied ($Voltage_{pp}$–kV) for air, Ar, He, Ar/H_2O, He/H_2O, He/O_2 discharge. (a) TDT power of the first discharge, voltage applied on the first discharge electrode (quartz tube). (b) TDT and ODT power of the PTFE tube discharge, voltage measured on the copper wire electrode. The error bars correspond to the standard deviation between multiple experiments (at least three).

begins to dissipate 3 W at 14 kV_{pp}, whereas all other discharges reach the same power level at voltages below 6 kV_{pp}.

Figure 6(b) compares the power dissipated in the PTFE tube by both ODT and TDT 2nd dis. The power dissipated in the tube for both devices varies at the same measured voltage on the wire, except for the Ar/H_2O and He discharges. It could indicate that, except for those two gases, the presence of a first discharge does change the parameters of the discharge in the tube, either by preheating the gas or by producing ROS in high amounts.

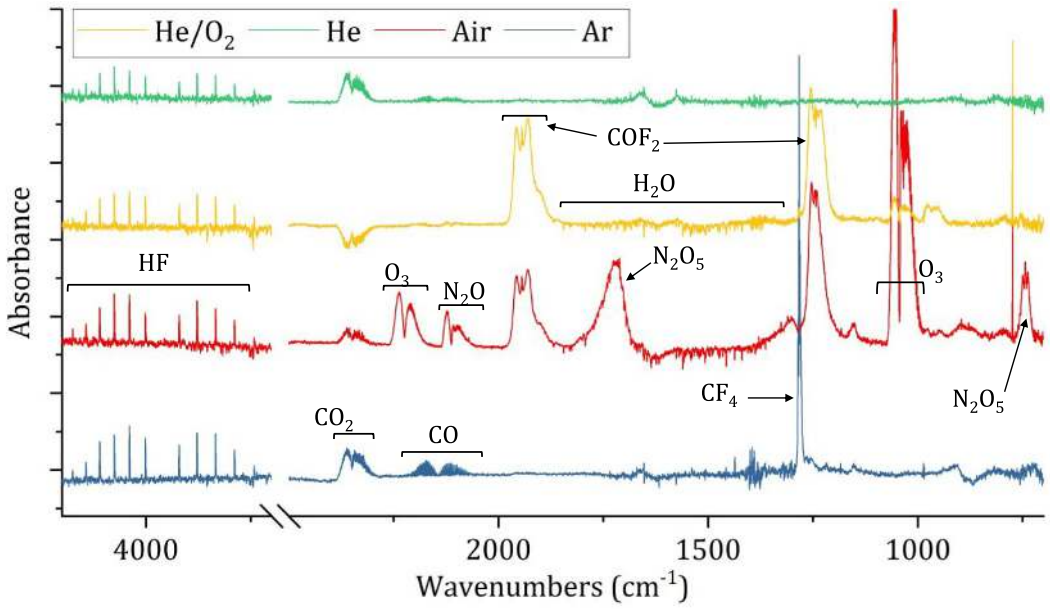

Figure 7. Typical FTIR spectra observed during He/O_2, He, Ar, and air discharge, regardless of the device (TDT or ODT), along with identification of the main absorption lines observed.

From the air curve of the TDT 2nd discharge, no power is dissipated in the tube, regardless of the applied voltage. This observation is consistent with the ODT measurements, where power dissipation in air starts above 5.8 kV, a voltage that is never reached in the TDT 2nd discharge due to excessive heating in the first discharge.

3.2. RONS production in the discharge

3.2.1. FTIR

The presence of RONS in the effluent of the discharge is of great importance, as they create a strongly oxidative medium effective at killing bacteria or degrading molecules on surfaces and in solution [13]. FTIR was therefore used to characterize the quantity of RONS produced during the discharges. Typical absorbance FTIR spectra obtained in the output gas of an He/O_2, He, air, and Ar discharge are presented in figure 7, along with typical RONS (O_3, NO, NO_2, N_2O_5), and PTFE degradation products (CO, CF_4, HF, and COF_2).

Figure 8 shows that pure gas discharges (Ar, He) do not produce RONS, and that all discharges react with the PTFE tube, producing fluorinated compounds due to PTFE degradation by ion bombardment and metastable reactions. The main degradation products observed in helium were HF and CO, whereas in Argon, CF_4 was also detected, and COF_2 was observed in air and He/O_2. The cumulated amount of F atoms being (one for HF, 4 for CF_4, and 2 for COF_2) increases with power and is higher for ODT than for TDT, except in the argon discharge. The presence of CO in a discharge that does not contain oxygen shows probable contamination by water, which could come from either the PTFE or from oxygen etched from the quartz tube of the TDT, which is supported by the higher amount of CO in the TDT.

In He/O_2, the TDT discharge produces an increasing concentration of ozone with increased power, reaching a maximum around 235 $\pm$ 1 ppm. In contrast, the ODT produces less ozone (109 $\pm$ 1 ppm), and its concentration decreases with increasing power. In the air discharge, the trends are inverted, with high ozone concentrations observed in the ODT discharge (1260 $\pm$ 1 ppm), along with low N_2O_5 concentrations (47 $\pm$ 2 ppm). On the contrary, the TDT discharge, which does not turn on in the PTFE tube and therefore dissipates all its power in the first discharge (quartz tube), produces 400 ppm of ozone at 5 W with 40 ppm of N_2O_5. The ozone production completely vanishes above 12 W, and the discharge produces an increasing amount of NO (226 $\pm$ 1 ppm at 30 W) and NO_2 (42 $\pm$ 1 ppm at 23 W). This regime change is a common behavior of N_2/O_2 DBD discharges, which is due to the destruction of ozone at high temperatures resulting from the increase in power density of the discharge at higher power levels. In the TDT air discharge, power is dissipated only during the first discharge, which is sufficient at 23 W to increase the gas temperature and suppress ozone production. Figure 9 presents the concentration in ppm of the various molecules produced in a 1.5 $l \cdot min^{-1}$ Ar, He, He/O_2, and air discharge for the ODT and the TDT, at 10 $\pm$ 2 W of power dissipated in the PTFE tube. The

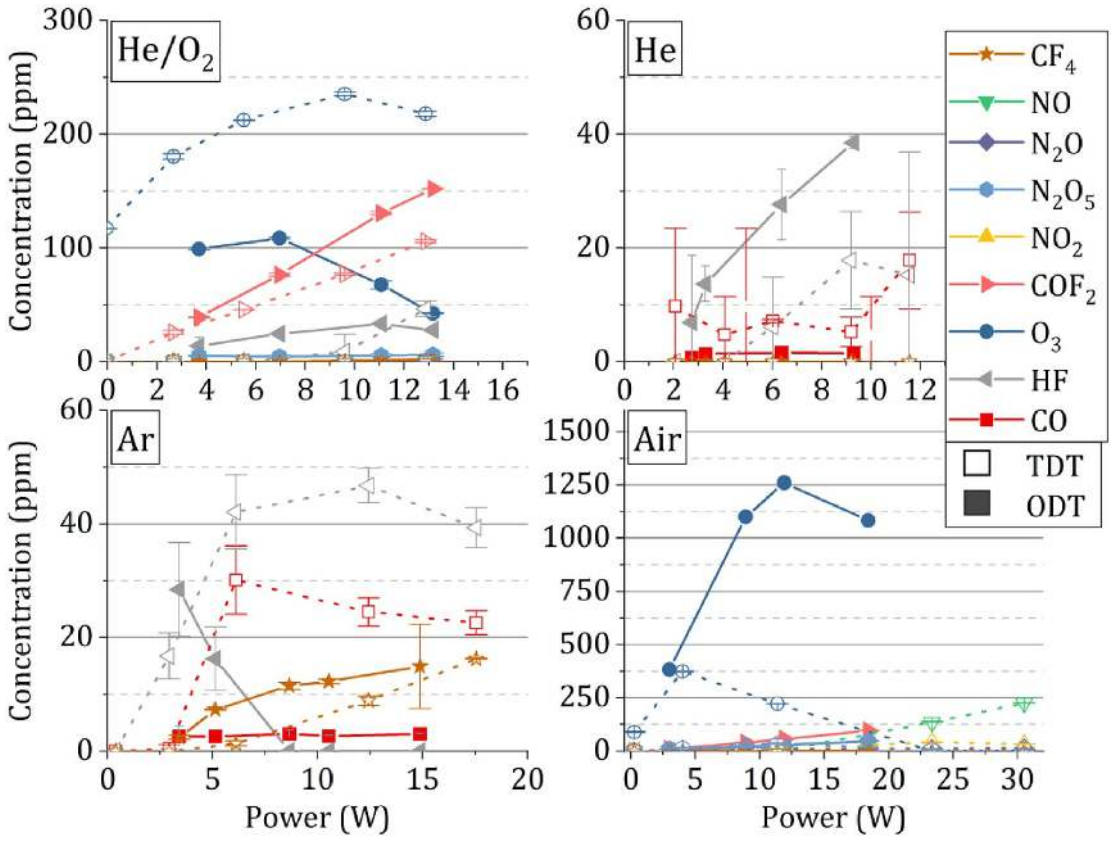

Figure 8. Concentration of CF_4, NO, NO_2, N_2O, N_2O_5, O_3, HF, CO and COF_2 (ppm) in TDT (hollow symbols) and ODT (plain symbols) discharges over the power (W) dissipated in the PTFE tube (2nd discharge in case of the TDT) for He/O_2, He, Ar, and Air ODT ($1.5\,l \cdot min^{-1}$), and the power dissipated in total for the TDT–air discharge.

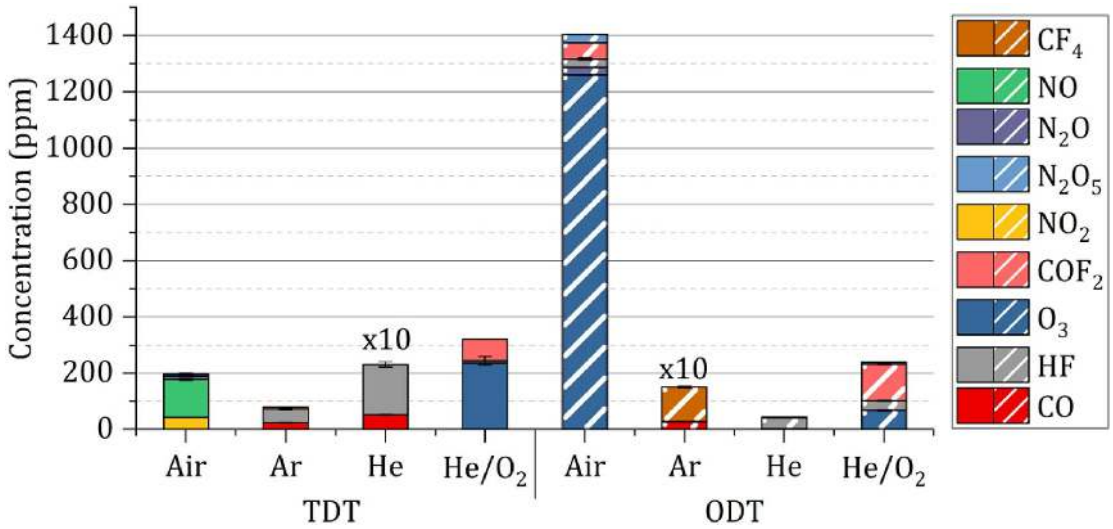

Figure 9. Gas concentration observed in the output gases from the ODT and TDT discharge for the tested gases without water saturation. $1.5\,l \cdot min^{-1}$ gas flow rates, around 10 ± 2 W of power in the PTFE tube for all discharge, except for the TDT–air discharge, with a power in the PTFE tube of 0.5 W.

TDT air discharge dissipates only 0.5 ± 0.2 W in the PTFE tube, for a total power of 23 ± 1 W. Ar/H_2O and He/H_2O are not presented due to the strong degradation of the spectra caused by water vapor absorption, which makes the accurate measurement of these species impossible. However, qualitative measurements show the presence of HF, CO, and COF2 in those discharges, in the ODT and the TDT (not presented), with a higher amount of HF and COF_2 under argon.

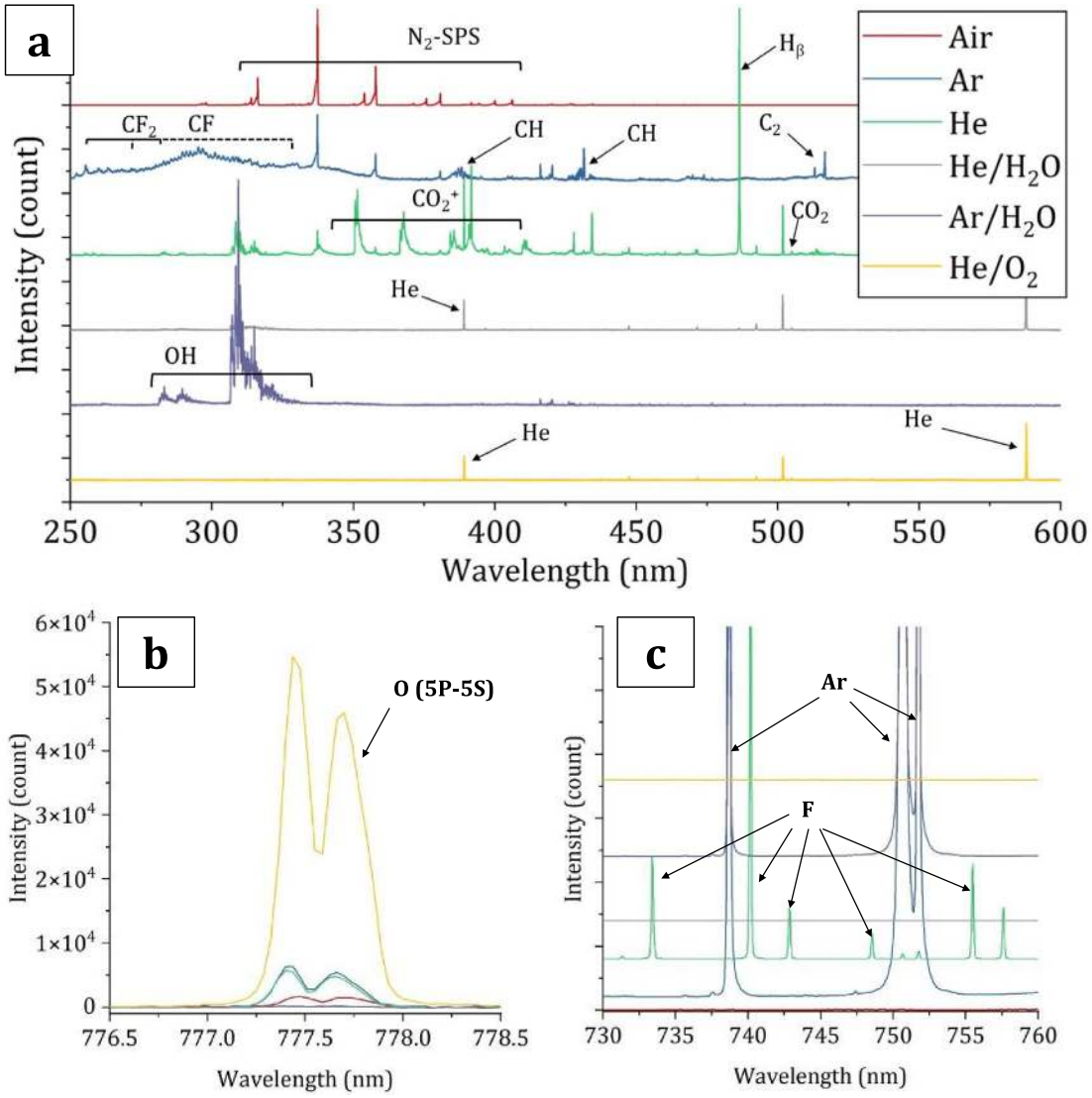

Figure 10. Typical spectra with identification of the main emission bands and lines observed in the PTFE tube during ODT He/O_2, Ar/H_2O, He/H_2O, He, Ar, and air discharge. All discharges are generated with an applied voltage of 4 kV, except for the air discharge, which is at 7 kV. (a) Emission spectra between 250 nm and 600 nm, (b) atomic oxygen emission, O($^5P \rightarrow {}^5S$), around 777.5 nm, (c) atomic fluorine and argon emission between 730 and 760 nm.

3.2.2. OES

The light emission from the plasma has been measured at the decontamination sample position and therefore reflects the plasma activity during the decontamination. Figure 10 presents the typical emission spectra for all gases tested between 250 nm and 600 nm. Each spectrum presents very different molecular bands and atomic lines. In air (only in ODT), the N_2(C–B) band is dominant and marks the presence of a discharge inside the tube. Conversely, during the TDT air discharge, no emission was recorded at any tested power (between 0 and 60 W). In both discharges containing water (He/H_2O and Ar/H_2O), a strong band of OH(A–X) is observed around 310 nm. The intensity of that band is compared to the H_2O_2 production in the next chapter. The rest of the spectrum is dominated by atomic emission from argon or helium. In pure helium or argon, the presence of PTFE fragments, namely CF, CF_2, CH, C_2, CO_2^+, and H_α, testifies to the interaction between the excited species, the PTFE walls, and the small water contamination providing oxygen and hydrogen atoms. It is interesting to note that in argon, due to the absence of the OH band, the fragments do not contain any oxygen atoms. On the other hand, in helium, the OH band is visible, along with CO_2 and CO_2^+, due to the oxidation of PTFE by OH radicals. In helium, the presence of atomic fluorine is also observed (figure 10(c)), which is not the case for any other discharge. This is due to the high-energy helium metastable (20 eV), which can break the PTFE and PTFE fragments, and release inorganic fluorine in the discharge. On the other hand, the argon metastable (11.5 eV) mainly breaks the polymer into monomers. This is correlated with the detection of CF_4 in an argon discharge, and only HF in helium. Finally, in He/O_2, the only notable emission is the

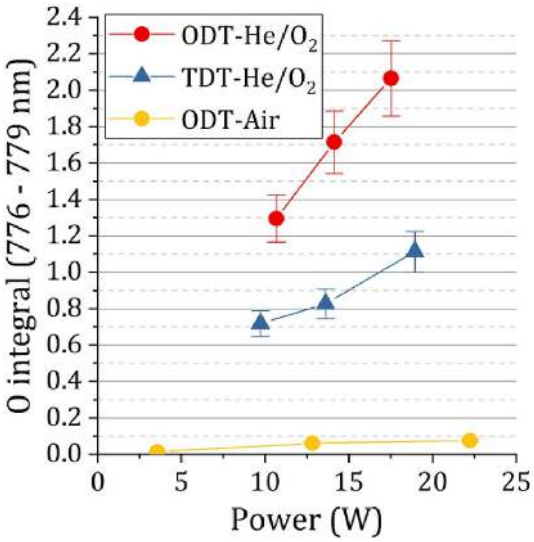

Figure 11. Atomic oxygen line intensity ($^5P \rightarrow {}^5S$) integrated between 776 and 779 nm over power dissipated in the PTFE tube, for an ODT and TDT–He/O_2 discharge and ODT–air discharge. 1.5 l · min^{-1} flow rate.

triplet of the atomic oxygen ($^5P \rightarrow {}^5S$) at 777.5 nm (figure 10(b)). This line is also detected in helium and argon due to water contamination, and in air due to the presence of oxygen in the discharge.

To compare the oxidative capability of ODT and TDT discharges in He/O_2 and air, we measured the atomic oxygen emission as a function of the power dissipated in the tube. In figure 11, the atomic oxygen emission increases with power dissipation for the three discharges, and the ODT generates twice as much O emission at the same power level as the TDT discharge.

3.2.3. H_2O_2 and OH radicals

H_2O_2 and OH radicals are linked by the reaction scheme ((R1)–(R5)) that produces H_2O_2 and OH(A–X) emission (R4) from H_2O in the He/H_2O and Ar/H_2O discharge,

$$H_2O + e^- \rightarrow OH + H + e^- \quad \text{(R1)}$$

$$OH + e^- \rightarrow OH(A) + e^- \quad \text{(R2)}$$

$$H_2O + Ar^* \rightarrow OH(A) + H + Ar \quad \text{(R3)}$$

$$OH(A) \rightarrow OH(X) + h\nu\,(\lambda_{h\nu} \approx 310\ \text{nm}) \quad \text{(R4)}$$

$$OH + OH + M \rightarrow H_2O_2 + M. \quad \text{(R5)}$$

Figures 12(a) and (b) compare the H_2O_2 production of the ODT and TDT discharge in Ar/H_2O and He/H_2O with the OH(A–X) emission over the power dissipated in the PTFE tube. In figure 12, it is clear that the Ar/H_2O discharge produce more H_2O_2 than the He/H_2O discharge, this can be attributed to the synergy between the argon metastable energy (11.5 eV) and the dissociation excitation of water (Dissociation energy ∼5.1 eV) that produce excited OH radicals (∼4.0 eV) and hydrogen atoms (R3) [50]. This is also visible in figure 12(b), with the argon discharge emission also higher than the helium discharge.

Between ODT and TDT, in terms of H_2O_2 production, they both produce the same amount until 9 W, after which the TDT produces more H_2O_2. This is not supported by the OH emission, as both produce the same emission at all power levels. The larger amount of H_2O_2 in the TDT could then originate from a supplementary production of H_2O_2 in the first discharge (which dissipates more power), not entirely destroyed by the second discharge (PTFE tube discharge). This could also explain the slightly lower OH intensity in the TDT, as part of the water has been converted into H_2O_2. In helium water discharges, both ODT and TDT produce a similar amount of H_2O_2 and present the same intensity of OH emission.

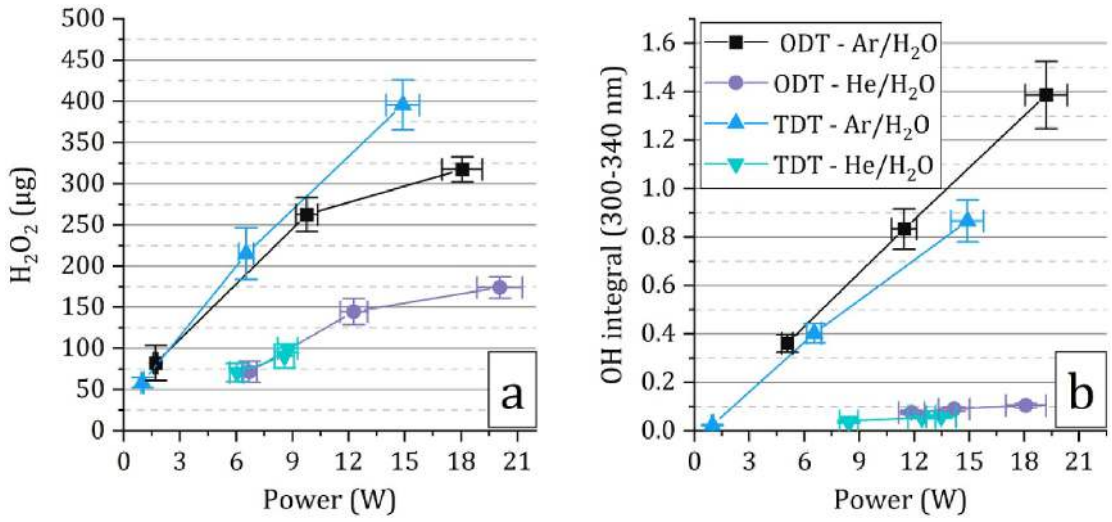

Figure 12. Comparison between H_2O_2 and OH for ODT and TDT discharges generated in 1.5 l · min^{-1} flow of argon and helium saturated with water vapor. (a) H_2O_2 (μg) produced by a 10 min discharge, (b) integral of the OH (A–X) emission band between 300 nm and 340 nm, as a function of the power dissipated in the PTFE tube (2nd discharge of the TDT).

3.3. Bacteria decontamination and biofilm removal

Bacterial decontamination assays were conducted to evaluate the decontamination and biofilm removal capability of the discharges and compare the ODT and the TDT. The discharge parameters were set at comparable levels, with 10 ± 1 W dissipated in the PTFE tube for all gases, except for the TDT air discharge, which was run at 23 ± 1 W of total power and less than 1 W of power dissipated in the PTFE tube. Those powers were selected to limit the heating of the PTFE tube to less than 50 °C, in compliance with the recommendation for the endoscope. The treatment time was fixed at five minutes of discharge.

Figure 13 presents the results of the decontamination assays, showing the biofilm left on the surface of the tube, in percentage of the control (measured by CV assay) and the viability of the bacteria (sample contaminated or decontaminated). The samples were decontaminated by nearly all discharges, both in ODT and TDT. The only ineffective discharge is the TDT–air discharge, which is not able to kill the bacteria. Although no statistical test was performed, the biofilm degradation capability shows no clear difference between the various treatments, with an average of 93 ± 11% of biofilm left on the surface for Ar, He, air, Ar/H_2O, and He/O_2. Only the He/H_2O-ODT shows a noticeably lower percentage, with 71 ± 6% of biofilm left, thus a reduction of nearly 30%.

4. Discussion

As shown by the characterization developed for the TDT and ODT, these two systems differ in terms of their electrical, chemical, and physical properties. Nevertheless, decontamination was achieved with a five-minute treatment for nearly all combinations of the devices and gases (Ar, Ar/H_2O, He/H_2O, He, He/O_2, and air). A decrease in the biofilm on the surface for some discharges was also observed.

4.1. Air discharges

The only exception to the decontamination was the TDT–Air discharge, which was unable to decontaminate the samples or decrease the quantity of biofilm left after treatment (95 ± 1% left after treatment). As shown by the electrical curves, the TDT–air discharge at 23 W of total power is unable to initiate a second discharge in the PTFE tube due to insufficient voltage being transmitted to the copper wire inside the PTFE tube (figure 6). This discharge produced RONS species, including NO, NO_2, and N_2O, with 135 ppm, 42 ppm, and 12 ppm, respectively (figure 9). NO and NO_2 in contact with the liquid trapped in the biofilm form NO_2^- and NO_3^-, decreasing the pH and reacting with proteins by nitration [51], therefore modifying the core biological processes of the bacteria. However, in a liquid solution, a pH lower than 4.7 must be reached to achieve bacterial reduction, as shown by Ikawa *et al* [12]. In our case, a small treatment time and a small concentration of NO and NO_2 in the gas were insufficient to decontaminate the sample.

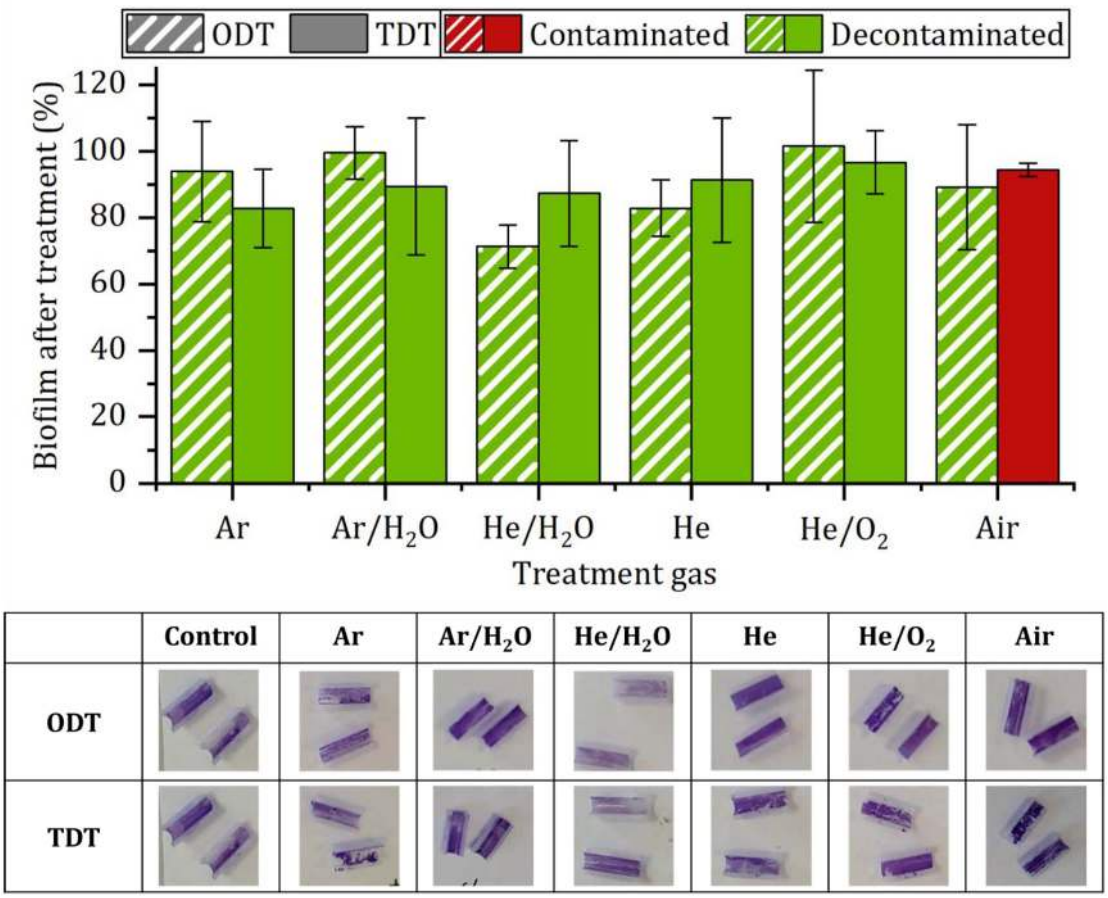

Figure 13. Biofilm left after treatment (crystal violet assay) on the sample after 5 min of the different plasma, and corresponding pictures of the samples halves after CV staining. 10 ± 2 W of power in the PTFE tube for all discharge, except for the TDT–air discharge with a power in the PTFE tube of 0.5 ± 0.2 W and a total power of 23 ± 1 W.

On the contrary, the ODT–Air treatment was effective at decontaminating the bacteria but was only slightly able to remove the biofilm from the surface, with 89 ± 19% of the biofilm still remaining on the surface. In contrast to the TDT–air, the ODT–air discharge has two advantages for decontamination: first, it generates the discharge directly in the PTFE tube, in contact with the sample, allowing the discharge to interact with the biofilm on the sample surface properly. The second advantage is the high ozone concentration (1260 ± 1 ppm) and a certain level of N_2O_5 (29 ± 1 ppm) in the gas (figure 9). The first is known for its biological activity at high concentrations and is already used to decontaminate wastewater, drinking water, or even medical devices [24, 26, 52]. N_2O_5, on the other hand, cannot react directly with the biofilm; instead, it dissolves and reacts with the water (in the biofilm) to acidify the biofilm (R6). It can also produce peroxynitrous acid (R7) and peroxynitric acid when combined with H_2O_2 ((R8) and (R9)), both of which have confirmed bactericidal activity [53],

$$N_2O_{5(aq)} + H_2O \rightarrow 2H^+_{(aq)} + 2NO_{3^-_{(aq)}} \quad \text{(R6)}$$

$$N_2O_5 + H_2O \rightarrow 2\ HOONO \quad \text{(R7)}$$

$$N_2O_{5(aq)} + H_2O \rightarrow NO_{3^-_{(aq)}} + NO_{2^+_{(aq)}} + H_2O \quad \text{(R8)}$$

$$NO_{2^+_{(aq)}} + H_2O_{2(aq)} \rightarrow HOONO_{2(aq)} + H^+. \quad \text{(R9)}$$

Those two reasons could explain why the ODT–air was able to decontaminate the sample, whereas the TDT–Air was not. It is interesting to note that the ODT–air was able to achieve decontamination in five minutes, whereas, according to the literature on ozone decontamination, multiple hours at a similar level

of ozone are required to achieve a reduction in bacterial activity [54]. Therefore, having the plasma directly in contact with the sample significantly reduces the decontamination time to only five minutes in our case, possibly due to the formation of peroxynitric and peroxynitrous acid in the biofilm.

4.2. Noble gases reactivity

The discharges containing pure noble gases (ODT–Ar, ODT–He, TDT–Ar, TDT–He) were all capable of decontaminating the samples regardless of the device used (figure 13). In these discharges, the argon and helium metastables react with the water contained in the biofilm, producing *in situ* OH radicals that can decontaminate the sample even in the absence of water or oxygen in the gas phase. For biofilm removal, there is no noticeable difference between the ODT and the TDT, or between argon and helium discharge. It should be noted that in both discharges, some amount of fluorinated compounds was observed, primarily by FTIR (COF_2, HF, and CF_4 in figure 9), but also through OES (CF, CF_2, and atomic F in figure 10). All those species are known for their high cellular toxicity and/or etching capabilities.

4.3. Oxygen in the discharge

The discharges containing helium and oxygen (He/O_2) are also able to decontaminate the sample, regardless of the device used; this ability is attributed to the large amount of atomic oxygen observed by OES (figure 10). On the other hand, they have similar biofilm-removal efficacy as air discharge, with $86 \pm 9\%$ and $100 \pm 20\%$ remaining after treatment for the He/O_2 TDT and ODT, respectively, and $89 \pm 19\%$ for the ODT–air (figure 13). This is in contradiction with the greater oxidative capability observed through the presence of a larger amount of COF_2 in the He/O_2 TDT (106 ± 1 ppm) and ODT (130 ± 1 ppm) than in the ODT–air (40 ± 1 ppm). Part of the atomic oxygen is also consumed by R10 to form ozone, with 1101 ± 17 ppm measured in air discharge and only 217 ± 2 ppm and 67 ± 3 ppm, respectively, in He/O_2, ODT, and TDT. This indicates that ozone is not effective at etching the biofilm in our system,

$$O + O_2 + M \rightarrow O_3 + M. \quad \text{(R10)}$$

The low biofilm removal efficacy of oxygen-containing discharges indicates that another species or process is required to remove the biofilm efficiently, possibly OH, as suggested by the higher biofilm removal efficacy of the He/H_2O treatment and its higher mineralization potential [26, 29].

4.4. Water-saturated discharges

For the two water-saturated gases (Ar/H_2O and He/H_2O), we have observed the production of H_2O_2 in effluent gas and the emission from OH radicals (around 310 nm) in discharges (figure 12). Both species have strong antibacterial activity, and in the full decontamination was achieved in every configuration. The biofilm removal capability was maximal for the ODT–He/H_2O, which reduced the biofilm by $29 \pm 6\%$. This was unexpected. Indeed, the OH emission intensity and H_2O_2 production are lower for discharges containing helium than for those containing argon, regardless of the setup design (figure 12). Helium discharges are known for their high concentration of helium metastable (20 eV), whose energy is high enough to efficiently break all the chemical bonds of organic materials, as confirmed by the release of atomic fluorine in our helium discharges (figure 10). On the other hand, argon metastables are primarily used for water dissociation, producing OH and H_2O_2 from water vapor ((R3), (R5)). We have also observed that the pure argon discharge releases large organic products from the surface (CF, CF_2, CF_4) and no atomic products. It suggests that it exists a synergy between the etching of the biofilm into atomic species by metastable helium and the presence of OH radicals in the gas phase to react with those species. This could yield a higher mineralization rate for helium compared to argon in the presence of water vapor and lower quantities of biofilm left on the surface after treatment (figure 13).

4.5. Fluorinated compounds

The detection of HF, COF_2, and even CF_4 in the effluent gases (figure 7), particularly when oxygen or water is added to the discharges, indicates a significant interaction between the plasma and the PTFE tube walls. Those species are known products of fluorinated polymer degradation by reactive species such as metastables, OH, or atomic oxygen [22, 55–57]. COF_2 and CF_4, which react with water to produce HF, to our knowledge have never been used for the decontamination of bacteria, even though it has already been suggested that their presence in the plasma effluent gas could help decontaminate biofilms [55]. Hence, their presence does not contribute to the overall decontamination efficiency of the plasma, but could help in the biofilm removal due to the etching capability of fluorinated compounds in

plasma discharges [23]. On the other hand, HF, COF_2, and CF_4 are highly toxic and corrosive gases that pose health and safety risks in confined environments. The maximum measured concentration for COF_2 (152 ± 1 ppm) and for HF (28 ± 2 ppm), in the effluent gas of the reactor ($1.5\ l \cdot min^{-1}$), would produce, in a well ventilated room ($40\ m^3 \cdot h^{-1} \cdot pers^{-1}$), a maximum fluorine concentration of 1 ppm, which is below the short-term exposure limit of 3 ppm recommended by the Eurofluor group [58]. Even if the health and environmental risk is low, it should be properly addressed for any clinical or industrial application.

4.6. Limits and future scope

Common, up-to-date disinfection techniques use mechanical action to reach HLD standards and fully remove the biofilm from the surface. They use multiple brushes and a pressurized flow of hot (>50 °C) disinfectant (glutaraldehyde) solutions over long treatment times to kill bacteria and remove biofilm. In the present study and in a precedent study using a similar setup [21], although the plasma could partially remove the biofilm, we were still unable to fully remove it from the entire surface of the tube. But we are not using any liquids or mechanical action to remove the biofilm, and we rely solely on the etching of the biofilm (mineralization), greatly diminishing hazardous (biological, chemical, and material) hardware and waste from the treatment, and even avoiding contact between the technical staff and the contaminated hardware.

As highlighted by the observation of equivalent decontamination and biofilm removal capabilities across all tested discharges, the characterization of RONS generation within the biofilm, both in the gas phase and in the biofilm, is essential to further comprehend the chemistry during CAP decontamination. However, the detection of RONS within the biofilm during treatment poses significant challenges. These reactive species generally possess short lifetimes and most likely react rapidly with the biomaterial, consequently preventing their accumulation in the biofilm and making *in-situ* detection extremely challenging.

Despite the different plasma chemistries, both systems successfully achieved complete bacterial decontamination after 5 min of treatment in nearly all gas compositions tested (Ar, He, He/O_2, Ar/H_2O, He/H_2O), with the notable exception of the TDT–air discharge, which failed to ignite within the PTFE tube and showed no biocidal activity. Further reducing treatment time could better differentiate among the various discharges, and implementing CFU assays would allow quantification of bacterial reduction, particularly in the absence of complete decontamination.

In the present study, the characterization of discharges was performed in the absence of a biofilm, in order to prevent the contamination of diagnostic equipment. However, replicating the FTIR and OES measurements during biofilm treatment would enable the detection of mineralization products (CO_2, CO, H_2O), particularly in pure Ar and He discharges, as well as previously undetected volatile organic compounds resulting from incomplete mineralization (CH, COH …). The ratio between these inorganic and organic products could then serve as an indicator to elucidate the chemical pathways involved in biofilm degradation.

The difference between Ar/H_2O and He/H_2O should be further investigated through a careful kinetic comparison of biofilm removal rates at longer treatment times. This would strengthen the hypothesis of synergy between helium metastables and OH radicals, which would be beneficial for biofilm matrix degradation and mineralization.

In addition, complementary analyzes of the biofilm surface using mass spectrometry, infrared spectroscopy, and chromatography could provide insights into changes in its chemical composition and structure, which would help to distinguish the effects of different discharge gases and the potential role of fluorinated compounds. The incorporation of these diagnostics in future studies will be crucial for advancing our understanding of plasma–biofilm interactions.

5. Conclusion

This study investigated the effectiveness of two DBD configurations, ODT and TDT, to decontaminate *P. aeruginosa* biofilms in long, flexible PTFE tubes, which mimic the working channels of endoscopes. This work assesses whether transporting reactive species generated upstream (TDT) could enhance bacterial inactivation and biofilm removal compared to a direct discharge (ODT) generated in contact with the contaminated surface.

Importantly, we have shown that the ODT configuration presents clear practical advantages over the TDT, especially in air. It requires fewer components, eliminates upstream discharge management, requires less energy, and can be easily integrated into endoscope reprocessing workflows. Moreover,

previous work using a similar ODT configuration with water-saturated argon demonstrated that extension of the treatment time from 5 to 30 min resulted in up to 80% biofilm removal [21], with minimal impact on the channel material [22].

In conclusion, this study confirms the feasibility of short-duration plasma treatment across a wide range of reactive gas mixtures for rapid, effective bacterial decontamination of long medical tubing. Overall, the technique's simplicity makes it a highly promising solution for clinical applications. In contrast to newly developed methods that require hazardous chemicals, lengthy reprocessing procedures, or single-use devices, this approach offers a safer and more sustainable alternative, reducing environmental impact by shortening the reprocessing chain and avoiding the use or generation of toxic waste. Further optimization of discharge duration and gas composition will be necessary to approach full biofilm removal without mechanical action, and realize a one-step, plasma-based endoscope reprocessing method.

Data availability statement

The data cannot be made publicly available upon publication because no suitable repository exists for hosting data in this field of study. The data that support the findings of this study are available upon reasonable request from the authors.

Acknowledgments

This work was supported by the ARC ('Action de Recherche Concertée') COSMIC projects, funded by the Université libre de Bruxelles (ULB).

ORCID iDs

Antoine Remy 0000-0003-4640-8071
Teo Serra 0000-0002-3094-8463
Amélie Bourgeois 0009-0006-0292-5375
Orianne Bastin 0000-0003-4993-3525

References

[1] Rutala W A 2017 Guideline for disinfection and sterilization in healthcare facilities: updated 2024 (available at: https://stacks.cdc.gov/view/cdc/47378)
[2] Kovaleva J, Peters F T M, van der Mei H C and Degener J E 2013 Transmission of infection by flexible gastrointestinal endoscopy and bronchoscopy *Clin. Microbiol. Rev.* **26** 231–54
[3] Larsen S, Russell R V, Mærkedahl A, Travis H S, Ockert L K and Ehlers L H 2020 Contamination rate of reusable patient-ready duodenoscopes used for endoscopic retrograde cholangiopancreatography (ercp): a systematic review and metaanalysis *Gastroenterology* **158** S–1004–S–1005
[4] Beilenhoff U *et al* 2017 Prevention of multidrug-resistant infections from contaminated duodenoscopes: position statement of the European society of gastrointestinal endoscopy (ESGE) and European society of gastroenterology nurses and associates (ESGENA) *Endoscopy* **49** 1098–106
[5] Beilenhoff U *et al* 2018 Reprocessing of flexible endoscopes and endoscopic accessories used in gastrointestinal endoscopy: position statement of the European society of gastrointestinal endoscopy (ESGE) and European society of gastroenterology nurses and associates (ESGENA)—up *Endoscopy* **50** 1205–34
[6] Society of Gastroenterology Nurses and Associates 2015 *Gas Sterilization of Endoscopes FAQs* (available at: www.sgna.org/Portals/0/Issues/PDF/Infection-Prevention/Gas%20Sterilization_FAQ_FINAL.pdf)
[7] Alfa M J, Ribeiro M M, da Costa Luciano C, Franca R, Olson N, DeGagne P and Singh H 2017 A novel polytetrafluoroethylene-channel model, which simulates low levels of culturable bacteria in buildup biofilm after repeated endoscope reprocessing *Gastrointest. Endosc.* **86** 442–451.e1
[8] Rauwers A W, Kwakman J A, Vos M C and Bruno M J 2019 Endoscope-associated infections: a brief summary of the current state and views toward the future *Tech. Gastrointest. Endosc.* **21** 150608
[9] Haugen S *et al* 2018 Duodenoscope surveillance sampling & culturing. Reducing the risks of infection, food drug adminstration
[10] Rutala W A and Weber D J 2024 Guideline for disinfection and sterilization in healthcare facilities, 2008 (Healthc. Infect. Control Pract. Advis. Comm.) pp 1–158 (available at: https://stacks.cdc.gov/view/cdc/47378) (Accessed 2 July 2024)
[11] Decroly G, Ben Hassen R, Achten W M J, Grimaldi D, Gaspard N, Devière J, Delchambre A and Nonclercq A 2023 Strong sustainability of medical technologies: a medical taboo? The case of disposable endoscopes *2023 45th Annual Int. Conf. IEEE Engineering in Medicine and Biology Society* (IEEE) pp 1–7
[12] Ikawa S, Kitano K and Hamaguchi S 2010 Effects of pH on bacterial inactivation in aqueous solutions due to low-temperature atmospheric pressure plasma application *Plasma Process. Polym.* **7** 33–42
[13] Mai-Prochnow A, Zhou R, Zhang T, (Ken) Ostrikov K, Mugunthan S, Rice S A and Cullen P J 2021 Interactions of plasma-activated water with biofilms: inactivation, dispersal effects and mechanisms of action *npj Biofilms Microbiomes* **7** 1–12
[14] Northage N, Shvalya V, Modic M, Juergens T, Eschborn S, Horsburgh M J and Walsh J L 2024 Evaluation of plasma activated liquids for the elimination of mixed species biofilms within endoscopic working channels *Sci. Rep.* **14** 1–11

[15] Alkawareek M Y, Algwari Q T, Laverty G, Gorman S P, Graham W G, O'Connell D and Gilmore B F 2012 Eradication of pseudomonas aeruginosa biofilms by atmospheric pressure non-thermal plasma *PLoS One* **7** 13–15
[16] Maho T *et al* 2021 Anti-bacterial action of plasma multi-jets in the context of chronic wound healing *Appl. Sci.* **11** 9598
[17] Matthes R, Bender C, Schlüter R, Koban I, Bussiahn R, Reuter S, Lademann J, Weltmann K D and Kramer A 2013 Antimicrobial efficacy of two surface barrier discharges with air plasma against *in vitro* biofilms *PLoS One* **8** 1–11
[18] Kuzminova A, Kretková T, Kylián O, Hanuš J, Khalakhan I, Prukner V, Doležalová E, Šimek M and Biederman H 2017 Etching of polymers, proteins and bacterial spores by atmospheric pressure DBD plasma in air *J. Phys. D: Appl. Phys.* **50** 135201
[19] Bhatt S, Mehta P, Chen C, Schneider C L, White L N, Chen H L and Kong M G 2019 Efficacy of low-temperature plasma-activated gas disinfection against biofilm on contaminated GI endoscope channels *Gastrointest. Endosc.* **89** 105–14
[20] Hervé R C, Kong M G, Bhatt S, Chen H L, Comoy E E, Deslys J P, Secker T J and Keevil C W 2023 Evaluation of cold atmospheric plasma for the decontamination of flexible endoscopes *J. Hosp. Infect.* **136** 100–9
[21] Remy A, Zveny J, Serra T, Lakhloufi D, Bourgeois A, Devière J, Botteaux A, Delchambre A, Reniers F and Nonclercq A 2025 Pseudomonas aeruginosa biofilm decontamination and removal by Ar/H_2O cold atmospheric plasma in endoscope-like tubing *J. Appl. Phys.* **58** 075202
[22] Zveny J, Remy A, Nickmilder P, Delchambre A, Nonclercq A, Leclère P and Reniers F 2024 Evaluating cold atmospheric plasma for endoscope decontamination: feasibility and impact analysis on PTFE surfaces *Plasma Med.* **14** 1–18
[23] Fridman A 2008 *Plasma Chemistry* (Cambridge University Press) (https://doi.org/10.1017/CBO9780511546075)
[24] Epelle E I, Macfarlane A, Cusack M, Burns A, Okolie J A, Mackay W, Rateb M and Yaseen M 2023 Ozone application in different industries: a review of recent developments *Chem. Eng. J.* **454** 140188
[25] Rakovsky S, Anachkov M and Georgiev V 2014 Reactions of ozone with hydrocarbons - kinetics and mechanism *Chemistry and Physics of Complex Materials* (Apple Academic Press) pp 225–34
[26] Sievers M 2011 Advanced oxidation processes *Treatise Water Science* (Elsevier) pp 377–408
[27] Alvárez' P M, Beltrán F J, Masa F J and Pocostales J P 2009 A comparison between catalytic ozonation and activated carbon adsorption/ozone-regeneration processes for wastewater treatment *Appl. Catal. B* **92** 393–400
[28] Fricke K, Steffen H, Von Woedtke T, Schröder K and Weltmann K D 2011 High rate etching of polymers by means of an atmospheric pressure plasma jet *Plasma Process. Polym.* **8** 51–58
[29] Legrini O, Oliveros E and Braun A M 1993 Photochemical processes for water treatment *Chem. Rev.* **93** 671–98
[30] Decauchy H, Pavy A, Camus M, Fouassier L and Dufour T 2022 Cold plasma endoscopy applied to biliary ducts: feasibility risk assessment on human-like and porcine models for the treatment of cholangiocarcinoma *J. Appl. Phys.* **55** 455401
[31] Soulier M, Vacek T, Géraud K and Dufour T 2025 Transferred plasma catheter for endotherapeutic applications: a parametric study of guided streamers dynamics *Phys. Plasmas* **32** 043506
[32] Reuter S, Von Woedtke T and Weltmann K D 2018 The kINPen - a review on physics and chemistry of the atmospheric pressure plasma jet and its applications *J. Phys. D: Appl. Phys.* **51** 233001
[33] Bastin O, Thulliez M, Merche D, Ozkan A, Nonclerq A, Delchambre A, Devière J and Reniers F 2019 Generation and transport of cold plasma in metres-long tubing for plasma medicine application in endoscopy *24th Int. Symp. Plasma Chem., Board of Directors of the Int. Plasma Chemistry Society (IPCS)* (*Naples*) p 4
[34] Bastin O, Thulliez M, Delchambre A, Devière J, Reniers F and Nonclercq A 2022 Analysis of a nano-pulsed DBD plasma jet for endoscopy and impact of excitation parameters *J. Appl. Phys.* **55** 415204
[35] Bastin O, Thuliez M, Servais J, Nonclercq A, Delchambre A, Hadefi A, Devière J and Reniers F 2020 Optical and electrical characteristics of an endoscopic DBD plasma jet *Plasma Med.* **10** 71–90
[36] Thulliez M, Bastin O, Nonclerq A, Delchambre A and Reniers F 2020 Comparison of sinusoidal and pulsed cold plasma transported in meters-long tubing on agarose gel models for application in endoscopy *8th Int. Conf. Plasma Medicine* p 1
[37] Thulliez M, Bastin O, Remy A, Nonclercq A, Devière J, Delchambre A and Reniers F 2022 Effect of gas flow on a helium/oxygen endoscopic plasma jet *J. Appl. Phys.* **55** 415202
[38] Thulliez M 2017 Feasibility study of a new endoscopic treatment using cold plasma
[39] Gordon I E *et al* 2022 The HITRAN2020 molecular spectroscopic database *J. Quant. Spectrosc. Radiat. Transfer* **277** 107949
[40] Machala Z, Tarabova B, Hensel K, Spetlikova E, Sikurova L and Lukes P 2013 Formation of ROS and RNS in water electro-sprayed through transient spark discharge in air and their bactericidal effects *Plasma Process. Polym.* **10** 649–59
[41] Pineau L, Roques C, Luc J and Michel G 1997 Automatic washer disinfector for flexible endoscopes: a new evaluation process *Endoscopy* **29** 372–9
[42] ISO 21871:2006(fr) 2006 *Microbiologie des aliments - méthode horizontale pour le dénombrement de Bacillus cereus présumés en petit nombre - technique du nombre le plus probable et méthode de recherche (International Organization for Standardization)Microbiologie des alimentsméthode horizontale pour le dénombrement de Bacillus cereus présumés en petit nombre-technique du nombre le plus probable et méthode de recherche (International Organization for Standardization)*
[43] Doern C D, Roberts A L, Hong W, Nelson J, Lukomski S, Swords W E and Reid S D 2009 Biofilm formation by group A Streptococcus: a role for the streptococcal regulator of virulence (Srv) and streptococcal cysteine protease (SpeB) *Microbiology* **155** 46–52
[44] Haney E F, Trimble M J, Cheng J T, Vallé Q and Hancock R E W 2018 Critical assessment of methods to quantify biofilm growth and evaluate antibiofilm activity of host defence peptides *Biomolecules* **8** 1–22
[45] Bastin O, Thulliez M, Serra T, Nyssen L, Fontaine T, Devière J, Delchambre A, Reniers F and Nonclercq A 2023 Electrical equivalent model of a long dielectric barrier discharge plasma jet for endoscopy *J. Appl. Phys.* **56** 1–43
[46] Osawa N and Yoshioka Y 2012 Generation of low-frequency homogeneous dielectric barrier discharge at atmospheric pressure *IEEE Trans. Plasma Sci.* **40** 2–8
[47] Gherardi N, Gouda G, Gat E, Ricard A and Massines F 2000 Transition from glow silent discharge to micro-discharges in nitrogen gas *Plasma Sources Sci. Technol.* **9** 340–6
[48] Enache I, Naudé N, Cambronne J P, Gherardi N and Massines F 2006 Electrical model of the atmospheric pressure glow discharge (APGD) in helium *Eur. Phys. J. Appl. Phys.* **33** 15–21
[49] Massines F, Rabehi A, Decomps P, Ben Gadri R, Ségur P and Mayoux C 1998 Experimental and theoretical study of a glow discharge at atmospheric pressure controlled by dielectric barrier *J. Appl. Phys.* **83** 2950–7
[50] Tabayashi K and Shobatake K 1988 Dissociative excitation of water by metastable rare gas atoms: Rg($^3P_0$,2) + H_2O→Rg + OH($A^2\Sigma^+$) +H (Rg=Ar,Kr) *J. Chem. Phys.* **88** 835–44
[51] Ji Y, Shi Y, Yang Y, Yang P, Wang L, Lu J, Li J, Zhou L, Ferronato C and Chovelon J-M 2019 Rethinking sulfate radical-based oxidation of nitrophenols: formation of toxic polynitrophenols, nitrated biphenyls and diphenyl ethers *J. Hazard. Mater.* **361** 152–61

[52] Rutala W A and Weber D J 2021 Disinfection and sterilization in health care facilities: an overview and current issues *Infect. Dis. Clin. North Am.* **35** 575–607
[53] Moldgy A, Nayak G, Aboubakr H A, Goyal S M and Bruggeman P J 2020 Inactivation of virus and bacteria using cold atmospheric pressure air plasmas and the role of reactive nitrogen species *J. Phys. D: Appl. Phys.* **53** 434004
[54] Thill S A and Spaltenstein M 2020 Toward efficient low-temperature ozone gas sterilization of medical devices *Ozone* **42** 386–98
[55] Xi W, Guo L, Liu D, Zhou R, Wang Z, Wang W, Liu Z, Wang X, (Ken) Ostrikov K and Rong M 2022 Upcycle hazard against other hazard: toxic fluorides from plasma fluoropolymer etching turn novel microbial disinfectants *J. Hazard. Mater.* **424** 127658
[56] Hubert J, Mertens J, Dufour T, Vandencasteele N, Reniers F, Viville P, Lazzaroni R, Raes M and Terryn H 2015 Synthesis and texturization processes of (super)-hydrophobic fluorinated surfaces by atmospheric plasma *J. Mater. Res.* **30** 3177–91
[57] Hubert J, Vandencasteele N, Mertens J, Viville P, Dufour T, Barroo C, Visart De Bocarmé T, Lazzaroni R and Reniers F 2015 Chemical and physical effects of the carrier gas on the atmospheric pressure PECVD of fluorinated precursors *Plasma Process. Polym.* **12** 1174–85
[58] European Technical Committee for Fluorine 2017 Guidelines in case of exposure with hydrogen fluoride (AHF) and hydrofluoric acid (HF) information for first aiders + health professionals, Eurofluor